CFD modeling and experimental study of combustion and nitric oxide emissions in hydrogen-fueled spark-ignition engine operating in a very wide range of EGR rates

Kosmadakis, GM; Rakopoulos, CD; Demuynck, J; De Paepe, M; Verhelst, S

In: INTERNATIONAL JOURNAL OF HYDROGEN ENERGY, 37 (14), pp. 10917-10934, 2012

http://dx.doi.org/10.1016/j.ijhydene.2012.04.067

CFD MODELING AND EXPERIMENTAL STUDY OF COMBUSTION AND NITRIC OXIDE EMISSIONS IN HYDROGEN-FUELED SPARK-IGNITION ENGINE OPERATING IN A VERY WIDE RANGE OF EGR

(COVER PAGE)

by

G.M. KOSMADAKIS : Research Associate, Dipl.Ing., M.Sc., Ph.D. (NTUA)

C.D. RAKOPOULOS : Professor of Internal Combustion Engines
Director of I.C. Engines Laboratory (NTUA)
Dipl.Ing., M.Sc., D.I.C., Ph.D.
(Imperial College of Science, Technology and Medicine, University of London)
M. ASME, M. N.Y.Acad.Sci., M. SAE, M. ASCE

J. DEMUYNCK* : Research Assistant, Dipl.Ing., M.Sc. (GHENT)
Ph.D. Candidate

M. DE PAEPE* : Professor of Applied Thermodynamics and Heat Transfer, Dipl.Ing., M.Sc., Ph.D. (GHENT)

S. VERHELST* : Professor of Internal Combustion Engines, Dipl.Ing., M.Sc., Ph.D. (GHENT)

Internal Combustion Engines Laboratory
Thermal Engineering Department, School of Mechanical Engineering
National Technical University of Athens (NTUA)
9 Heroon Polytechniou St., Zografou Campus, 15780 Athens, Greece
Tel.: +30 210 7723529, Fax: +30 210 7723531
E-mail: cdrakops@central.ntua.gr

*Department of Flow, Heat and Combustion Mechanics
Ghent University (GHENT)
Sint-Pietersnieuwstraat 41, B-9000 Ghent, Belgium

Submitted for publication to the International Journal of
HYDROGEN ENERGY, Elsevier Science
Editor-in-Chief: Professor T. Nejat Veziroglu

Experimental and CFD modeling study of combustion and nitric oxide emissions in hydrogen-fueled spark-ignition engine operating in a very wide range of EGR rates

G.M. Kosmadakis[a], C.D. Rakopoulos[a,*], J. Demuynck[b], M. De Paepe[b], S. Verhelst[b]

[a] *Internal Combustion Engines Laboratory, Thermal Engineering Department, School of Mechanical Engineering, National Technical University of Athens, 9 Heroon Polytechniou St., Zografou Campus, 15780 Athens, Greece*
[b] *Department of Flow, Heat and Combustion Mechanics, Ghent University, Sint-Pietersnieuwstraat 41, B-9000 Ghent, Belgium*

ABSTRACT

In the current work, the variation of EGR rates is investigated in a hydrogen-fueled, spark-ignition engine. This technique is followed in order to control the engine load and decrease the exhaust nitrogen oxides emissions. The external EGR is varied in the very wide range of 12% up to 47% (by mass), where in each test case the in-cylinder mixture is stoichiometric, diluted with the appropriate EGR rate. The operation of this engine is explored using measured data with the aid of a validated CFD code. Moreover, a new residual gas term existing in the expression of the hydrogen laminar flame speed, which has been derived from a one-dimensional chemical kinetics code, is tested in a real application for appraising its capabilities. The investigation conducted provides insight on the performance and indicated efficiency of the engine, the combustion processes, and the emissions of nitrogen oxides. More precisely, an experimental study has been deployed with the aim to identify the characteristics of such a technique, using very high EGR rates, focusing on the combustion phenomena. At the same time, the CFD results are compared with the corresponding measured ones, in order to evaluate the CFD code under such non-conventional operating conditions and to test a recent expression for the residual gas term included in the hydrogen laminar flame speed expression. It is revealed that the combustion takes place in few degrees of crank angle, especially at high engine loads (low EGR rates), whereas the exhaust nitrogen oxides emissions are significantly decreased in comparison to the use of lean mixtures for controlling the engine load. Additionally, the recent expression of the residual gas term, which has been tested and incorporated in the CFD code, seems to be adequate for the calculation of combustion phenomena in highly diluted, with EGR, hydrogen-fueled spark-ignition engines, as for every EGR rate tested (even for the higher ones) the computational results are compared in good terms with the measured data.

Keywords: Hydrogen; Spark-ignition engine; EGR; Combustion; NO emissions.

[*] Corresponding author. Tel.: +30 210 7723529; Fax: +30 210 7723531.
E-mail address: cdrakops@central.ntua.gr (C.D. Rakopoulos).

Nomenclature

A	calibration constant in turbulent flame speed expression
$D_{T,u}$	thermal diffusivity of the unburned mixture, m^2/s
f	residual gas fraction by volume, %
F	residual gas correction expression
k	turbulent kinetic energy (per unit mass), m^2/s^2
LHV_{H_2}	lower heating value of hydrogen, kJ/kg
L_t	turbulent integral length scale, m
m_{H_2}	inlet hydrogen mass, kg
$\dot{m}_{EGR}$	EGR mass flow rate, kg/s
$\dot{m}_{air}$	air mass flow rate, kg/s
$\dot{m}_{H_2}$	hydrogen mass flow rate, kg/s
n_{gi}	gross indicated efficiency, %
P	pressure, N/m^2
P_{IVC}	pressure at inlet valve closure, N/m^2
P_o	reference pressure, N/m^2
Q_{H_2}	heat of combustion, J
r_k	local flame kernel radius, m
S_{cr}	source term due to crevice flows
S_ϕ	source term
t	time, s
T	temperature, K
T_o	reference temperature, K
T_u	unburned gas temperature, K
u_f	flame propagation velocity, m/s
u_l	laminar flame speed, m/s
u_{l0}	laminar flame speed at reference conditions, m/s
u_t	turbulent flame speed, m/s
u'	rms turbulent velocity, m/s
$\vec{u}$	velocity vector, m/s
V	cylinder volume, m^3
V_s	swept volume, m^3
W_{gi}	gross indicated work, J

W_i indicated work, J

Greek symbols

Γ_ϕ diffusion coefficient, kg/m s

ε turbulent dissipation rate (per unit mass), m^2/s^3

λ relative air-to-fuel ratio

ρ density, kg/m^3

ρ_b burned gas density, kg/m^3

ρ_u unburned gas density, kg/m^3

τ_c characteristic conversion time, s

τ_l laminar kinetics time, s

τ_t turbulent mixing time, s

φ fuel-to-air equivalence ratio or (simply) equivalence ratio

ϕ generalized variable

Abbreviations

ABDC after bottom dead center

ATDC after top dead center

BBDC before bottom dead center

BDC bottom dead center

CFD computational fluid dynamics

CFR cooperative fuel research

COV coefficient of variance

CR compression ratio

^{o}CA degrees of crank angle

EGR exhaust gas recirculation

EOI end of injection

EVC exhaust valve closing

EVO exhaust valve opening

HCCI homogeneous charge compression ignition

IMEP indicated mean effective pressure

IT ignition timing

IVC inlet valve closure

IVO inlet valve opening

MBT	minimum spark advance for best torque
MFB	mass fraction burned
NO	nitric oxide
NO_x	nitrogen oxides
PFI	port fuel injection
PISO	pressure implicit splitting of operators
rms	root mean square
rpm	revolutions per minute
SI	spark-ignition
TDC	top dead center
TWC	three-way-catalyst
UEGO	universal exhaust gas oxygen

1. Introduction

One type of engine showing high research interest is the spark-ignition engine running on hydrogen, for which appropriate experimental test-benches are developed, in order to investigate the combustion processes and their performance under different operating conditions and strategies [1-7], as well as the various in-cylinder processes taking place [8-12]. Apart from these experimental investigations, numerical tools are also developed [8,13-16], which can further assist in the understanding of the various processes taking place in those engines. Especially, the results obtained from computational fluid dynamics (CFD) codes [8,16], which describe in a more fundamental way the in-cylinder processes [17,18], can identify at a local level the coupling of the relevant transport phenomena.

One method of regulating the engine load and decreasing the exhaust nitrogen oxides (NO_x), is the use of exhaust gas recirculation (EGR). While in diesel and HCCI engines the use of large quantities of EGR is a common practice [19-23], in gasoline spark-ignition (SI) engines significantly lower EGR rates are used, due to the severe decrease of flame speed. Recently, attention is paid to the use of larger EGR rates in spark-ignition engines using fuels other than gasoline, such as natural gas, hydrogen etc. [24-27]. More specifically, in hydrogen-fueled spark ignition engines the use of EGR aims at decreasing the exhaust nitrogen oxides (NO_x) and regulating the engine load without the need of throttling. The first target can be directly achieved, since the fresh mixture diluted with exhaust gases possesses a higher specific heat capacity, thus decreasing

the maximum combustion temperature. On the other hand, the second target (control of engine load) can be achieved due to the wide flammability limits of hydrogen by appropriately adjusting the EGR rate up to a certain point, beyond which significant cycle-to-cycle variations as well as significant quantities of unburned hydrogen in the exhaust appear, witnessing a low combustion efficiency [28,29].

In the present study both experimental and numerical investigations are accomplished, for identifying in detail some critical processes taking place in a hydrogen-fueled spark-ignition engine. More specifically, measurements have been conducted on a single-cylinder, Cooperative Fuel Research (CFR) engine, at a single compression ratio and for a wide range of external EGR rates (from around 12% up to 47% by mass). In each case, the minimum spark advance for best torque (MBT) timing was used. The scope is to investigate the combustion phenomena occurring in the cylinder, especially for the higher EGR rates. To assist with this, an in-house CFD code has been applied for the simulation of the in-cylinder processes and validated at those conditions, by comparing some critical calculated values with the measured data, such as the engine's performance and nitric oxide (NO) exhaust emissions for various EGR rates. Then, the computational results are further processed in order to have a more detailed view of the in-cylinder processes. It should be pointed out that a recent expression of the residuals gas term [30] included in the hydrogen laminar flame speed, valid for even high EGR rates, is incorporated in the combustion model of the CFD code and is tested in a real application.

2. Experimental data

2.1. Test engine and equipment

The experimental data used in the present study concern measurements on a CFR engine (flat piston/cylinder head), operating at a constant engine speed equal to 600 rpm (maintained by an electric motor) and equipped with a sequential port-fuel injection (PFI) system. The load of the engine is regulated with the variation of the EGR rate, while the fresh intake air/hydrogen mixture is always stoichiometric (φ=1). In the present study, these external EGR rates are varied from 12% to around 47% (by mass). Fuel injection and ignition timing are controlled by a 'MoTeC M4Pro' unit [2]. The main specifications of this engine are given in Table 1.

Air is admitted in the engine through a buffer vessel to obtain a more or less constant air flow in order to enable air mass flow measurements, as the current engine is a

single-cylinder one. Another flow meter is installed in the fuel line between the hydrogen storage and the injector. These flow meters (measuring in Nm^3/h) are both manufactured by 'Bronkhorst' and allow calculation of the air/fuel ratio, which is also possible with the oxygen sensor placed in the exhaust pipe. The injector manufactured by 'Teleflex Ltd' is designed to deliver large volumes of gas and is mounted in the intake duct, 40 cm away from the inlet valve of engine. The injector is placed at a 45 degree angle to the inlet air flow, which has been found to be beneficial for the efficiency [31]. With a programmable engine management system, the start of injection and the injection duration can be easily controlled, while the injection pressure is regulated by a valve on the H_2 storage bottle. A piezo-electric high pressure transducer (Kistler 701A pressure sensor) is located in the cylinder head, flush with the wall. Another piezo-electric transducer is located in the exhaust duct, just after the exhaust valve. A piezo-resistive pressure transducer is also installed for pressure referencing (in order to have reliable pressure initial conditions, P_{IVC}, for the CFD simulations) and is located in the intake duct, 8 cm away from the inlet valve. A Crank Angle sensor gives pulses every 1° CA (or with an interpolator at 0.5, 0.25 or 0.1 °CA).

2.2. EGR experimental tests

For the current EGR tests, the test-rig is completed with an EGR line with regulation valve and a heat exchanger. Originally, a water condensate discharge in the EGR line was also used [32,33], which has been dropped out in the current study since with its use the resulted dry recirculated exhaust gas possessed a lower specific heat capacity, thus increasing the combustion temperatures and the NO_x emissions as well.

The test rig set-up that was adopted here is shown in Fig. 1. A boiler was installed in a closed loop water flow to control the EGR temperature, which should be maintained below 70 ^oC to avoid abnormal combustion (knock and backfire) [3]. A throttle valve was installed in the air inlet duct as an extra device to regulate the amount of EGR, as also shown in Fig. 1.

In the exhaust pipe a three-way-catalyst (TWC) is mounted, just after the EGR line, with a metallic substrate (type 'Bosal'), which has a light-off temperature of about 280–300 ^oC and a maximum temperature of 800–850 ^oC, according to the manufacturer. It should be stressed that the exhaust gas temperature of the CFR engine is rather low [18], so it is necessary to place the TWC as close as possible to the engine exhaust valve, in order to operate with a high conversion efficiency. A sampling of the exhaust

gases before and after the TWC was provided, and several temperature sensors were mounted in the inlet, exhaust, and EGR lines. The exhaust gases after the TWC are guided through a damper vessel and a water lock. The height of the water column can be altered to obtain a counter pressure in the exhaust line, thus increasing control over the amounts of EGR.

All tests are implemented with a fixed engine speed of 600 rpm, and the end of injection (EOI) is always kept constant at BDC, so that all fuel is injected before the closing of the inlet valve at 26 ^{o}CA ABDC. The injection pressure is kept at 2 bar gauge.

The procedure for obtaining stoichiometric hydrogen-air mixtures with variable EGR rates is explained next. The engine is started at a certain lean operating condition (for example at λ=1.6, i.e. φ=0.625), with the EGR valve fully closed so that no exhaust gas is recirculated in the inlet (EGR=0%). By gradually opening the EGR valve, while keeping the inlet hydrogen flow rate constant, less air is admitted into the cylinder, since it is displaced by recirculated exhaust gas, and the mixture of hydrogen and air becomes richer until finally the stoichiometric condition (λ=1, i.e. φ=1) is obtained at a certain EGR ratio (in other words, at a specific EGR valve opening). This stoichiometric condition can be tracked by assuming that no fuel (H_2) and oxygen is present in the exhaust gases (tracked by an oxygen sensor at the exhaust, UEGO), since these consist almost exclusively of vapor water (H_2O) and nitrogen (N_2). To conduct other tests with another EGR ratio, the engine has to start from another lean condition (for example, λ=1.8 / φ=0.555 or λ=1.4 / φ=0.71) and follow a similar procedure.

Apart from the procedure followed in the current study and described previously, stoichiometric hydrogen-air mixtures with variable EGR rates can also be obtained by using the throttle valve in the air inlet line. This regulation can be done with hardly any flow losses (decrease of the inlet pressure), since by closing the throttle valve and restricting the air flow, the pressure after the valve decreases, which results in an increase of the EGR flow (additional EGR is sucked), maintaining the atmospheric pressure before the inlet valve and inside the cylinder (disregarding the pressure waves by the opening and closing of the inlet valve) [32,33].

The EGR ratio (by mass) is defined as the mass flow rate of EGR, $\dot{m}_{EGR}$, divided by the sum of mass flows rates of EGR, admitted air and injected fuel, $\dot{m}_{EGR} + \dot{m}_{air} + \dot{m}_{H_2}$, using Eq. (1), and can be calculated using the measured flow rates and temperatures, by assuming complete combustion.

$$EGR\,(by\ mass) = \frac{\dot{m}_{EGR}}{\dot{m}_{EGR} + \dot{m}_{air} + \dot{m}_{H_2}} \quad (1)$$

An alternative way of calculating the EGR ratio is from the measured CO_2 concentration in the intake (after mixing the EGR with the fresh mixture of air/fuel) and in the exhaust. This cannot be followed here, as only traces of CO_2 are present in the EGR (less than 0.1% by vol.), originating from the oxidation of the lubrication oil [34]. Another possibility is to use the measured O_2 concentrations in the intake and the exhaust [5], although the oxygen concentration at the exhaust is very low, due to the stoichiometric mixtures used. Different methods are currently investigated for determining the EGR rate in hydrogen-fuelled internal combustion engines by the UGent team, with the aim of finding the most accurate one.

Owing to the valve timing (IVO after EVC, i.e. no valve overlapping, see Table 1) some internal EGR also exists. This is not taken into account in the calculated EGR ratios of the experiments, by using Eq. (1).

2.3. Measured data and conditions investigated

The measured data that will be elaborated here concern the inlet mass flow rates of air and hydrogen, the cylinder pressure traces, the NO_x emissions (which will be considered equal to NO emissions from now on) as measured by a gas analyzer manufactured by 'Maihak', and the inlet and exhaust gas temperatures at various locations. These data are measured for different operating conditions when varying the external EGR rates (from around 12 to 47%), always keeping a stoichiometric air/hydrogen mixture (φ=1). The compression ratio (CR) is constant and equal to 9:1, while the ignition-timing is set equal to MBT for every case. The conditions investigated are shown in Table 2 (the EGR percentage refers to the external one only).

2.4. Variable EGR rates versus lean mixtures strategy

The regulation of the engine load with varying the EGR rate can be directly compared to the strategy of 'mixture leaning' by using lean mixtures (regulation of equivalence ratio, by varying the H_2 injection duration during the intake stoke while always ending at BDC). These two strategies have different operational characteristics, and they can be compared not for the same equivalence ratio, but for the same hydrogen flow rate and/or indicated mean effective pressure (IMEP). The measured hydrogen flow rates for the same engine load are depicted in Fig. 2 for both strategies, showing also the

corresponding EGR rates (variable EGR strategy) and equivalence ratio (mixture leaning strategy). The case of zero EGR rate is also shown for reference.

Next, the coefficient of variance (COV) of indicated mean effective pressure (IMEP) is investigated for both strategies. This value is actually an index of the combustion stability and the cyclic variation of each operating condition [5,35], calculated here for 30 consecutive engine cycles. This coefficient should hold low values, indicating normal engine operation; it is calculated by Eq. (2) and shown in Fig. 3 for various EGR rates. In the same figure, the COV values are also shown when the regulation of the engine load is achieved with the use of lean mixtures (variation of equivalence ratio).

$$COV_{IMEP}\,(\%) = \frac{1}{N}\frac{\sqrt{\sum_{i=1}^{N}\left(IMEP - IMEP_{mean}\right)^2}}{IMEP_{mean}}100 \qquad (2)$$

where $IMEP=W_i/V_s$, with W_i the indicated work (in Joules) and V_s the swept volume (m^3), and $IMEP_{mean}$ the mean value of $IMEP$, averaged over the N consecutive engine cycles (N equals to 30).

When using lean mixtures for the regulation of the engine load, an almost constant low COV is noticed (lower than 1%). On the other hand, with the use of various EGR rates, an even lower COV is observed at high loads (EGR lower than 25%), which leads to increased combustion stability [35]. But as the EGR increases over 42%, unacceptable values occur, leading to a high cyclic variation due to the high-dilution and the increased combustion duration (low flame speed). According to the criterion of combustion stability, the maximum tolerance of this engine to EGR at the rotational speed of 600 rpm can be set at almost 45% (resulting COV equal to around 3%, see Fig. 3). This is, however, a very high EGR rate. Then, if the internal EGR is also taken into account, it can be concluded that about half of the in-cylinder trapped gas at IVC is composed of already burned gas (residual gas) and still the engine operates satisfactorily with relatively low combustion instability and cyclic variation.

It should be mentioned that when using the mixture leaning strategy for the regulation of the engine load, significantly higher NO emissions are measured, ranging from 4400 to 180 ppm as the load decreases.

Concerning the unburned hydrogen at the exhaust, it is maintained lower than around 0.4% by vol. According to the measured data, the hydrogen at the exhaust is increased from around 0.2% by vol. at low EGR to around 0.4% by vol. at high EGR, having unfortunately a high measurement error and strong fluctuations due to the low values.

These values are by far below the flammability limit of hydrogen in air (around 4% by vol.). It should be, however, noticed that when using lean mixtures to control the engine load, even lower unburned hydrogen values can be measured at the exhaust (around half).

3. Numerical model

Next, the numerical model applied will be briefly described, since more detailed information can be found in previous studies [18,36].

3.1. CFD model

The firing version of the CFD code developed by the first two authors can simulate three-dimensional curvilinear domains, using the finite volume method in a collocated grid. It has been validated against measured data in previously published works [18,36], showing that it is capable of simulating adequately the power cycle of hydrogen-fueled, spark-ignition engines.

The in-house CFD code developed incorporates the RNG k–ε turbulence model [37] with some slight modifications to introduce the compressibility of a fluid in generalized coordinates, as described in Ref. [38]. It solves the transport equations for the conservation of mass, momentum, chemical species and energy, Eq. (3), as suggested in Ref. [39].

$$\frac{\partial(\rho\phi)}{\partial t} + \nabla\cdot\left(\rho\vec{u}\phi\right) = \nabla\cdot\left(\Gamma_\phi\nabla(\phi)\right) + S_\phi + S_{cr} \tag{3}$$

The second source term shown in Eq. (3), S_{cr}, represents the effect of the phenomenological crevice model incorporated in the CFD code [40]. Furthermore, the source terms of the turbulent kinetic energy and its dissipation are the same as in Ref. [41].

The wall-heat flux correlation developed in a previous work [41] is used for the simulation of the heat transfer mechanism and the calculation of the heat loss. Its formulation is based on the compressible version of the standard law-of-the-wall [42], and it includes not only a pressure term, which has been also shown in [43,44] to give more accurate results, but also a combustion term. Its validation under firing conditions has been accomplished in [18].

Further details of this in-house CFD model, concerning the pressure-correction algorithm used (PISO) [38], the turbulence model, the mesh generation model, the

phenomenological crevice model, as well as a detailed evaluation and validation of the developed CFD model under both motoring and firing conditions, can be found in previous published papers by the first two authors [18,36,40,41,44,45].

3.2. Combustion model

In the next subsections the combustion model developed and incorporated in the CFD code will be briefly presented, as applied for the simulation of hydrogen-fueled, spark-ignition engines. Only its basic features will be outlined, as its detailed presentation is provided elsewhere [18,36]. A more detailed elaboration will concern only the expression of the residual gas term (being the backbone of this work), existing in the expression of the hydrogen laminar flame speed [30].

3.2.1. Laminar and turbulent burning velocities (ignition and main stage of combustion)

In the developed combustion model, a correlation of the hydrogen laminar flame speed (u_l) is used [36]. After investigating various correlations for engine relevant conditions found in the literature [7,30], which additionally include stretch effects, a recently published correlation was implemented in the combustion model [46], whose general expression is shown in Eq. (4).

$$u_l = u_{l0}\left(\frac{T_u}{T_0}\right)^{\alpha}\left(\frac{P}{P_0}\right)^{\beta} F \tag{4}$$

where u_{lo} is the laminar flame speed at reference conditions (P_0, T_0), T_u the unburned gas temperature, α and β are the temperature and pressure exponent respectively [46], and F the correction expression due to the residual gas.

This correlation is used in order to track the computational cells in which the flame has propagated (partly or fully) during the ignition phase [36]. This is accomplished with the calculation of the local flame kernel radius (r_k), by approximating the flame propagation velocity with the laminar flame speed ($u_f \approx u_l$), since the characteristic dimension of the flame is considered to be smaller than the prevailing turbulence eddies during the ignition phase. The local flame kernel radius is calculated, by solving Eq. (5) after an appropriate temporal discretization [36].

$$\frac{dr_k}{dt} = \frac{\rho_u}{\rho_b} u_f = \frac{\rho_u}{\rho_b} u_l \tag{5}$$

where ρ_u, ρ_b the unburned and burned gas density respectively.

For the initialization of Eq. (5) at the start of ignition, it is considered that the initial flame kernel diameter is equal to 1 mm, which is approximately equal to the spark-plug gaps more often used in spark-ignition engines. The ignition energy supplied by the spark-plug is simulated by adding energy to the appropriate computational cell located at the point where the spark plug is placed (offset from the cylinder axis by around 30 mm). The spark duration is equal to 5 degrees CA and the supplied spark energy to the combustible mixture is 10 mJ, being a quite low value, since it also incorporates the heat energy loss to the electrodes; no additional model has been implemented to simulate this process, due to the great uncertainty of the exact shape, temperature and transient effects near the spark electrodes. The end of the ignition process and the transition to the turbulent combustion is determined by the time instant that the flame kernel radius exceeds a specific constant value (critical radius), equal to 4 mm [8]. More details concerning the incorporation of the laminar flame speed into the combustion model and the description of the ignition model can be found in Ref. [36].

The laminar flame speed is used not only during the ignition process, when the initial flame kernel approximately propagates with its laminar flame speed [8], but also during the turbulent flame development phase, when the laminar flame speed is inserted in the expression of the turbulent burning velocity. In the developed combustion model the turbulent flame speed (u_t) is used, in order to track the computational cells in which the flame has propagated (partly or fully) during the main stages of combustion after the ignition phase. The expression incorporated is the one proposed in Refs. [47,48], where only one calibration constant 'A' needs to be tuned. This tuning process has been accomplished in the evaluation study of this combustion model [36], where the calibration constant has been found to be equal to 0.8. In the present study this constant holds the same value for every case examined. The expression describing the turbulent flame speed is given by Eq. (6), which has been shown to give reliable results, especially at low/moderate turbulence (when $u' < u_l$, as is the case in most hydrogen-fueled SI engines) [47,48].

$$u_t = A(u')^{3/4} u_l^{1/2} D_{T,u}^{-1/4} L_t^{1/4} + u_l \tag{6}$$

where A is the only calibration constant, u' the rms turbulent velocity given by $u' = \sqrt{2k/3}$, $D_{T,u}$ the thermal diffusivity of the unburned mixture, and L_t the turbulent integral length scale given by $L_t = 0.37\,(u')^3/\varepsilon$.

The calculation of the local flame kernel radius is implemented by discretizing and solving a similar expression as Eq. (5), with the difference that the turbulent flame speed is used instead of the laminar one ($u_f \approx u_t$).

Further details concerning the implementation of this turbulent burning velocity expression in the combustion model developed and the description of the turbulent flame development phase can be found in Ref. [36].

3.2.2. Residual gas term

Recently, a new correlation of the residual gas term has been suggested for the hydrogen laminar flame speed, which is derived from a large range of EGR rates [30]. The calculated values of this expression have a correct physical meaning at high EGR rates, contrary to the previous one proposed in the literature [1], which is widely used and calculates negative values at these conditions. In the present study, where significantly high EGR rates are used (maximum external EGR equal to around 47% by mass), reliable expressions should be used to calculate adequately the combustion phenomena.

To take into account the effect of residual gas dilution, the laminar flame speed function is multiplied by a relevant correction expression '*F*' (see Eq. (4)). The expression used up to now, describing the effect of the residual gas fraction, is depicted in Eq. (7) [1].

$$F(\gamma,\lambda) = (1-\gamma f) \tag{7}$$

where $\gamma = 2.715 - \frac{0.5}{\lambda}$, λ is the relative air-to-fuel ratio, and f the residual gas fraction by volume, valid for f values from 0% to 30% by vol. [1].

The new expression suggested, which is valid for f from 0% to 50% by vol. [30], is given in Eq. (8), with a maximum value of unity (for f equal to zero).

$$\begin{aligned} F(T,f,\lambda,P) = {} & c_1 + c_2\frac{T}{T_o} + c_3\frac{P}{P_o} + c_4\lambda + c_5 f + c_6\left(\frac{P}{P_o}\right)^2 + c_7\left(\frac{T}{T_o}\right)^2 + c_8\lambda^2 + c_9 f^2 + \\ & + c_{10}\frac{T}{T_o}\frac{P}{P_o} + c_{11}\frac{P}{P_o}\lambda + c_{12} f\,\lambda + \frac{c_{13}}{\lambda} + \frac{c_{14}}{\lambda}\frac{T}{T_o} + c_{15}\frac{P_o}{P}\frac{T}{T_o} + c_{16}\frac{T}{T_o} f^3 + \\ & + c_{17}\frac{P}{P_o} f^3 + c_{18}\lambda f^3 + c_{19}\frac{P}{P_o}\frac{1}{\lambda} + c_{20}\frac{P}{P_o} f + c_{21} f\frac{T}{T_o} \end{aligned} \tag{8}$$

where T_o=300 K, P_o=1 bar, and the coefficients c_i (i=1 to 21) are given in Table 3 [30].

It should be stressed that the residual gas is composed of the internal (burned gas remained in the cylinder) and external EGR (recirculated exhaust gas).

In Fig. 4 the calculated values of the two aforementioned expressions (Eqs. (7) and (8)) are shown, for three representative combinations of pressure and unburned gas temperature (10 bar/600 K, 20 bar/700 K, 30 bar/800 K) and for two equivalence ratios (φ=1 and 0.75).

Fig. 4 shows that negative values are calculated (non-physical results) with the previous term (Eq. (7)), when the EGR is increased beyond 40% by vol. On the contrary, with the new term (Eq. (8)) always positive values are calculated for EGR lower than 55% (maximum validity range of 50%); this is satisfactory for the requirements of the present study and most of the relevant studies found in the literature [5,14,49].

3.2.3. Reaction rates calculation

The basic sub-model incorporated in the developed CFD code for the calculation of the reaction rates is the characteristic conversion time-scale method. This sub-model uses a characteristic time-scale (τ_c), which is the sum of the laminar conversion time (τ_l) and the turbulent mixing time (τ_t), and dictates to what extent the combustible gas of each computational cell (partly or fully swept by the flame front) has reached its chemical equilibrium in a predefined time step. This methodology is followed for the calculation of the reaction rates of all chemical species taken into consideration here, namely H_2, O_2, N_2, H_2O, H, O, N, and OH, except for the nitric oxide (NO), which is kinetically controlled and its reaction rate will be discussed in the next sub-section.

The methodology followed originates from the work of Abraham et al. [50], which has gone through some major improvements ever since [51] and has been also extended to other types of engines [52,53]. Recently, it has been formulated for the simulation of hydrogen-fueled spark-ignition engines and validated against experimental data, while further details concerning the calculation of the reaction rates with the use of the characteristic conversion time-scale method can be found in Ref. [36].

3.2.4. NO formation modeling

It has been shown that the reaction rate of the nitric oxide (NO) is kinetically controlled, governed primarily by three kinetic reactions known as the extended Zeldovich mechanism (thermal NO) [54].

The methodology followed is the same as the one presented in detail in [55]. The most usual set of constants for the reaction rates of the three chemical equations considered is also used in the present study, which is the one reported in Ref. [55]. Nevertheless, these constants were derived for hydrocarbon fuels, and so their uncertainty (which is already quite high) increases when applied for the calculation of the nitric oxide reaction rates in the case of a carbon-free fuel [16].

3.3. Computational details

In the present study some initial and boundary conditions are provided from the experimental data, such as the pressure at IVC, and the inlet air and hydrogen flow rates. For the rest of the required conditions, reliable estimations are used. The initial flow field is calculated by considering an initial low swirl ratio at IVC equal to 1.5, since the inlet valve is unshrouded [53]. The initial turbulence properties are the same as the ones derived from a relevant work concerning the same engine [53], and are held constant for every case examined here, since the engine speed is kept constant as well. More specifically, the initial turbulent velocity (u') at IVC is equal to 5.16 m/s, giving a mass-weighted average rms turbulent velocity at TDC equal to around 0.80 m/s, although the latter value slightly changes with the EGR rate. The initial gas temperature at IVC is estimated according to the measured inlet/exhaust/recirculated flow rates and temperatures and is varied from 370 to 405 K, as the EGR rate decreases [56], while the wall temperature is varied from 405 to 450 K, according to previous experimental investigations concerning the same engine and similar operating conditions [2,18].

The estimation of the internal residual gas mass fraction plays a minor role in the value of the laminar flame speed in the current study, since a significant amount of external EGR already exists. Nevertheless, estimations concerning the values of internal residual gas are obtained from the works reported in [57,58], combined with the measured air and hydrogen inlet flow rates. No overlapping period of the inlet and exhaust valves exists in this specific engine, thus making the estimation of the amount of internal residual gas rather simpler.

For the simulations to be reliable and most importantly to calculate adequately the NO exhaust emissions, multiple (consecutive) closed engine cycles have been simulated. This procedure is briefly described next. The first simulation cycle considers that the trapped gas in the cylinder is only composed of H_2, O_2, N_2, and H_2O. At the end of this simulation (at EVO) the mass fraction of each species is calculated, so that the internal

and external EGR is composed of nine species in total, which is actually the input to the second simulation cycle. This EGR (internal and external) is mixed up with the fresh mixture (hydrogen and air) in order for the second simulation cycle to begin, where at its end (at EVO) an updated mass fraction for all nine species is calculated. Then a third simulation cycle is initiated and so on until this procedure goes to convergence, characterized by the invariance of the NO mass fraction at EVO from a cycle to the next. It should be pointed out that performance values remain actually the same during these multiple cycles, whereas the exhaust emissions significantly change from cycle to cycle, especially for the higher EGR rates where high quantities of NO are recirculated, requiring more cycles to converge. By following this procedure, the initial in-cylinder mixture at IVC from the second cycle onwards is composed of all nine species. Fig. 5 shows the calculated NO mass fraction at EVO for each simulation cycle (medium and high EGR rates). For the low EGR cases, 2 to 3 simulation cycles (runs) are sufficient for this procedure to converge, while for the higher EGR cases up to 12 cycles (runs) may be required. It should be mentioned that during this iterative procedure, the initial gas temperature in the simulations is kept constant, since only the low species mass fractions actually change over engine cycles (even for high EGR rates).

Concerning the computational mesh used, previous relevant studies [36,40], together with a parametric study using the firing version of the developed CFD code, have shown that the most reliable mesh, providing adequate accuracy and keeping the required CPU time relative low, is the one having (40x40x40) grid lines along each axis respectively. The computational mesh at the beginning of the simulations (IVC) is shown in Fig. 6, where the location of the spark-plug is also depicted. The grid-spacing along the x- and y-axis is very uniform and equal to around 2 mm, while the initial grid-spacing along the z-axis (axial) is around 3 mm, decreasing as the piston moves towards TDC. The methodology of adding or removing mesh layers, according to the piston's movement, is the same as the one described in Ref. [40].

The computational time step used is kept low and equal to 0.5 ^{o}CA, since it has been shown that this is small enough to provide time-step independent solutions [40], even for low rotational speeds. During the combustion period, initiating from the ignition timing and afterwards, the time step is further decreased and becomes equal to 0.1 ^{o}CA, as in Ref. [8]. This methodology is followed in order to increase the accuracy of the computational results and also to enhance the stability of the code, since during each

time step the variation of the cylinder pressure and temperature is large, especially for the higher load cases (low EGR).

Finally, the only calibration constant used in the in-house CFD code exists in the expression of the turbulent flame speed, and retains the value A=0.8 (as mentioned previously in subsection 3.2.1.) for all cases examined [36].

4. Results and discussion

4.1. Test cases examined

The operating conditions of the CFR engine investigated in the present study concern the variation of the external EGR rates. For all cases examined the spark-timing is set to its MBT value, and the engine speed is kept constant at 600 rpm. Table 2 gives the matrix of all test cases examined.

4.2. Validation of the CFD code for various EGR rates

The in-house CFD code is first validated for various EGR rates, taking into consideration both performance and emission parameters, by comparing the calculated results with the measured data. Then, the numerical results will be further processed, aiming at the investigation of the in-cylinder processes at such operating conditions.

4.2.1. Cylinder pressure and performance

The validation procedure first considers the comparison of the calculated cylinder pressure traces and net heat release rate [18] with the measurements. This comparison is depicted in Fig. 7.

It can be observed that for every EGR rate, the differences of the calculated results from the measured data are kept low, especially at low EGR rates. Moreover, the peak pressure is predicted with high accuracy, together with the pressure prior to spark-ignition and during the expansion phase [18]. For EGR rates higher than 42% the numerical predictions are not so precise, since during the early expansion stroke the calculated pressure is under-predicted, a fact that can be partly attributed to the uncertainties of the laminar flame speed for such conditions.

Furthermore, it is observed that the peak cylinder pressure acquires relatively high values and decreases slightly as the EGR rate increases, up to around 35%. For even

higher EGR rates a significant decrease of the peak pressure is observed, which is attributed to the low burning velocity (see Fig. 4) and is well captured by the CFD code.

Concerning the net heat release rate, the timing of the calculated peak value is slightly advanced in comparison with the measured one, while at absolute values the peak values match. Moreover, the combustion duration is well captured by the CFD code, while this duration increases for higher EGR rates, which is presented with more detail in another section of this study.

The validation of the CFD code explores further the gross IMEP and indicated efficiency of the engine during the closed part of the engine cycle. These performance values are calculated from Eqs. (9) to (11) [18], and the comparison of calculated values with the corresponding measured ones for various EGR rates can be seen in Fig. 8.

$$W_{gi} = \int_{IVC}^{EVO} P\,dV \tag{9}$$

$$IMEP = \frac{W_{gi}}{V_s} \tag{10}$$

$$n_{gi} = \frac{W_{gi}}{Q_{H_2}} = \frac{W_{gi}}{m_{H_2}\,LHV_{H_2}} \tag{11}$$

where W_{gi} the gross indicated work, P the cylinder pressure, V the cylinder volume, V_s the swept volume, n_{gi} the gross indicated efficiency, Q_{H_2} the heat of combustion, m_{H_2} the trapped hydrogen mass per engine cycle, and LHV_{H_2} the lower heating value of hydrogen, equal to 120 MJ/kg [1].

As the EGR rates increase, the engine load decreases and IMEP takes values from 5.9 down to 3.8 bar. On the other hand, the indicated efficiency increases as the load decreases, due to low heat transfer and lower combustion products dissociation [18,59], up to around 42% EGR. Afterwards, the efficiency radically decreases, especially because of low combustion efficiency, since significant unburned hydrogen exists at the exhaust [18]. These trends of IMEP and indicated efficiency are successfully predicted by the CFD code, with the differences being very small for all cases examined and significantly lower than the experimental error [2].

Therefore, it can be concluded that the CFD code developed can adequately predict the performance of a hydrogen-fueled, spark-ignition engine using variable EGR rates for the regulation of the engine load, especially for low/mid EGR rates. Moreover, the expression of the residual gas term that has been used and incorporated into the

hydrogen laminar flame speed correlation seems to be capable of providing reliable flame speed values, in order to calculate the combustion phenomena.

4.2.2. Exhaust NO emissions

The validation of the CFD code continues with the investigation of the exhaust NO emissions before the three-way catalyst. This comparison is depicted in Fig. 9. It should be pointed out that with the multiple simulation cycles that were considered in the current study (see subsection 4.2 above), the exhaust NO emissions significantly varied from cycle to cycle until their final value is converged. This procedure requires more than 3 calculation cycles, especially for higher EGR rates.

It is generally observed that the match of these emissions is quite good for EGR rates lower than 20%, although some differences in absolute terms are observed (lower than 50%). For higher EGR rates there is an important discrepancy, which is attributed to a great extent to the incapability of the Zeldovich-mechanism's set of constants (and their high uncertainty) [54] to calculate the nitric oxide emissions with high accuracy [36]. This is under investigation by the authors, planning to use in future works an updated set of constants, specially developed for hydrogen fuel [16]. Nevertheless, the trend of the emissions is captured adequately as the EGR rate varies, although in absolute values the comparison is not very accurate.

Moreover, it seems that the use of high EGR rates (low engine loads) leads to important discrepancy in absolute values between the calculated results and the measured data, and larger than when lean mixtures are used for the regulation of the engine load. This can be verified, by taking into consideration Ref. [18], in which the mixture leaning strategy (no EGR) was used and the minimum engine load was kept higher than in the present study, providing more reliable NO predictions than in the present study.

In order to provide a more detailed view of the in-cylinder processes, and to try to explain the reason for this high difference between the measured and calculated NO emissions, the in-cylinder images of Fig. 10 are shown next, which can help identify the NO production mechanisms, especially at high diluted mixtures. These images show the evolution of the spatial temperature field, together with the NO mass fraction distribution, for selected time instants and planes after the spark-timing for three different levels of EGR (low/mid/high). One should notice the different contour range for the temperature and the NO mass fraction, as the EGR rate changes, while the upper right hand side

plane in each image is the one crossing the spark-plug. It can be observed with higher detail, how the NO production strictly follows the temperature variation, also witnessing the location of the flame propagating from the spark-plug location towards the cylinder walls.

From these images it is observed that for the low EGR rate case (high engine load), the flame has covered the whole combustion chamber at 20 ^{o}CA after the spark-timing. At that moment the NO mass fraction has its peak value, and starts to decrease afterwards. For the mid engine load case (mid EGR rate), the flame propagation velocity is similar to the high engine load, since at 20 ^{o}CA after the spark-timing the flame has almost covered the whole cylinder, but the NO continues to be produced until around 32 ^{o}CA after the spark-timing, when the local gas temperature has just started to decline from its high values of around 2200 K. For the low engine load case (high EGR rate), the burning velocity is very low, since at 44 ^{o}CA after the spark-timing the flame still propagates towards the chamber walls, and the local temperature is very low (peak value slightly higher than 1700 K). Due to the low local temperatures, the calculated NO mass fraction is very low, but lower than the measured values as well. Possibly, an updated set of constants of the Zeldovich mechanism could resolve this inaccuracy, which is investigated at the moment, as was already mentioned.

It should be pointed out, that for the mid/low engine load (mid/high EGR rate) the higher NO mass fraction is observed near the spark-plug and at the center of the combustion chamber for the whole combustion period, where the prevailing temperatures are also higher, but a significant in-cylinder NO mass fraction stratification exists at the end of combustion. On the contrary, an almost uniform temperature and NO spatial distribution are evident for the high engine load case (low EGR rate).

Concluding, it has been shown that the developed CFD code can adequately predict the performance and the trend of exhaust nitric oxide emissions of a hydrogen-fueled spark-ignition engine, where the engine load is regulated with the variation of the external EGR.

4.3. Investigation of mass fraction burned and combustion duration

After the validation of the CFD code has been implemented, the computational results are further processed in order to investigate the in-cylinder combustion phenomena of this spark-ignition engine. This analysis is initiated with the combustion duration and the hydrogen mass fraction burned, for each case considered in the present study.

The combustion duration can be calculated from the normalization of the integral of the gross heat release rate [5]. However, in order to have more accurate results, this duration will be calculated based on the reaction rates calculated directly from the combustion model of the CFD code. By doing so, the hydrogen mass fraction burned can be then derived; it is shown in Fig. 11 for various EGR rates (note the different scale of the horizontal axis).

It can be observed that the slope of the mass fraction burned is significantly higher for EGR rates lower than 30%, although the ignition-timing is retarded in these cases (see Table 2) and the unburned gas temperature at the spark-timing is lower. Moreover, for EGR rates higher than 40% the combustion duration is much higher, since combustion is completed in more than 40 ^{o}CA, whereas for the low EGR cases only a few degrees CA are required (less than 15 ^{o}CA) for the whole combustion process.

In order to investigate the combustion duration, the whole combustion period is split into two sub-periods. The first one is the flame development period (usually referred to as ignition delay period as well [14]), which is defined here as the time period in crank angle degrees from spark-ignition until the mass fraction burned (MFB) reaches the value of 5% (0-5% MFB). The second sub-period is the main combustion period, which in a similar way is defined as the time period in crank angle degrees just after the flame development period (from 5% MFB) until the mass fraction burned reaches the value of 99% (5-99% MFB). Fig. 12 shows the two aforementioned time periods for various EGR rates, as well as the total combustion duration (0-99% MFB).

It can be observed that both combustion periods have relatively low values for low EGR rates, whereas they are substantially increased as the EGR becomes higher than around 35% by mass. At the maximum EGR rate investigated here (around 47%) the whole combustion process takes place in almost 80 ^{o}CA, being around 8 times longer than the one for the minimum EGR rate. In this case combustion is far from a constant volume one [18,59,60], leading to decreased indicated efficiency (see Fig. 8).

It should be mentioned that the reduced indicated efficiency at high EGR rates is attributed not only to the increased combustion duration, as explained before, but also to the increased unburned hydrogen at the exhaust, which will be presented in the next sub-section.

4.4. Unburned hydrogen at the exhaust

The unburned hydrogen at the exhaust is responsible for the decrease of the indicated efficiency, since some fuel traces are not burned, decreasing the combustion efficiency [18] and increasing the COV of IMEP, especially at high EGR rates as shown previously in Fig. 3. Moreover, in Ref. [18] it was shown that for lean mixtures the unburned hydrogen at the exhaust becomes a significant reason for decreasing the combustion efficiency, as the engine load decreases (lower equivalence ratio used). This also is true here, where the engine load is regulated with the variation of EGR. Figure 13 shows the calculated unburned hydrogen at the EVO for variable EGR rates, obtained from the processing of the computational results of the CFD code.

As the EGR rates are increased, the unburned hydrogen at the exhaust is increased, proving the poor combustion efficiency [18]. It should be mentioned that the computed values are in the same range as the measured ones, mentioned previously; a direct comparison cannot be attempted though, due to the high measurement error for such low concentrations.

4.5. Investigation of the flame speeds and flame propagation

As mentioned in Section 3, a recent expression of the residual gas term [30], included in the hydrogen laminar flame speed correlation, is considered in the present study, which is valid for a wide range of residual gas fractions (up to 50% by vol.). Some simulation attempts that have been made with the previous expression, shown in Eq. (7) [1], failed to provide reliable results, especially for higher EGR rates, since negative values of the residual gas term have been calculated, which is of course unrealistic. These negative values are set equal to zero in the computations of the combustion model, for avoiding code divergence. In these cases a laminar and turbulent flame speed equal to zero is calculated, and the flame does not propagate (zero heat release).

The calculated values of the laminar and turbulent flame speeds for various EGR rates are shown in Fig. 14, while the flame radius is depicted in Fig. 15. It should be pointed out that these calculated values are obtained from the computational cells, which are located at an axial direction crossing the spark-plug, and until the flame reaches the piston.

It can be observed from Fig. 14 that the mixture laminar flame speed is substantially higher when the EGR rates are low, as expected. The differences in the calculated values are mainly attributed to the strong variation of the EGR rates (residual gas term of Eq. (8)). A minor effect of these differences emanates from the different mixture

temperature and pressure at the spark-timing, due to the different MBT values [36]. For example, the gas temperature/pressure at the spark-timing is around 800 K/17.4 bar for the case with the lower EGR rate, 765 K/16.9 bar for EGR equal to 34%, and 730 K/16.1 bar for the highest EGR considered. The turbulent flame speed has a similar trend for variable EGR rates, since it includes the laminar flame speed in its expression [36], while it also takes into account the local turbulent properties. For the lowest EGR case, due to the retarded spark-timing, the turbulence level has decayed (u'=0.72 m/s), and this is why lower values are calculated in comparison to the 18% EGR case (u'=0.76 m/s).

Concerning the flame radius depicted in Fig. 15, the flame reaches the piston in less time (fewer crank angle degrees, since the engine speed is held constant) for lower EGR rates, due to the higher burning velocity. Moreover, the maximum radius observed is around 12 mm, which is somehow lower than the height of the cylinder dead volume (equal to 14.27 mm), taking into consideration the position of the spark-plug (1 mm lower than the cylinder head) and the position the piston possesses at the instant the flame impinges on the piston wall.

The flame propagates with a speed equal to its laminar burning velocity [36] up to a flame radius equal to 4 mm, which corresponds to almost one third of its total radius. This brings an additional computational need for using a reliable expression of the laminar flame speed and its residual gas term, in order to be able to predict with high accuracy the operation, performance, and exhaust emissions of such highly diluted engines, with EGR rates reaching nearly values of 50%.

5. Summary and conclusions

An experimental investigation has been conducted concerning a hydrogen-fueled, spark-ignition engine, operating with external EGR rates varying in a very wide range, reaching even 47% by mass. The experimental procedure involved the measurement of the cylinder pressure traces, the inlet air and hydrogen flow rates, and additionally the tailpipe exhaust NO emissions for all cases examined.

The numerical results obtained from an in-house CFD code were first compared with the available measurements in order to validate its combustion model, which incorporates a very recent expression of the residual gas term inserted into the laminar flame speed formula. This validation process includes the comparison of performance and exhaust nitric oxide (NO) emission values. Then, the numerical results were further

processed in order to investigate, in more detail, the combustion processes of such highly diluted mixtures.

More specifically, the mass fraction burned was examined for all cases, showing that for high EGR rates the combustion process lasts much longer. This fact can be better identified with the investigation of the combustion durations, where for the highest EGR rate the whole combustion process lasts almost 80 ^{o}CA. On the contrary, for the lowest EGR rate combustion is completed in just 10 ^{o}CA. This increased duration for the highly diluted mixtures brings a reduced indicated efficiency, together with an increase of the unburned hydrogen at the exhaust, due to the low combustion temperatures.

One important aspect of the current work was the test of a recent expression of the residual gas term, incorporated in the expression of the laminar flame speed. This new expression is valid for large quantities of residual gas, and with its use reliable results were obtained. Additionally, the values of the laminar and turbulent flame speeds together with the flame radius have been computed during the flame propagation process, showing the differences that exist in the flame speed during the ignition phase and the turbulent flame development phase.

This in-depth investigation shows that the promising hydrogen-fuelled, spark-ignition engines can operate under the EGR strategy for the regulation of engine load, with reduced exhaust emissions. Even with an EGR rate equal to nearly 50% the engine could operate, albeit with a low efficiency. Indeed this strategy is proved very successful, especially at lower EGR rates, where the engine operates certainly in a stable way and the unburned hydrogen at the exhaust is kept under acceptable limits.

Furthermore, the computational results show that the CFD code developed can simulate with good accuracy such in-cylinder processes, especially for low/mid EGR rates, predicting adequately the measured performance and exhaust NO emissions. For the more reliable prediction of the latter ones, the constants of the Zeldovich-mechanism are under investigation and planned to be substituted, in a future communication, with a different set of parameters, applicable for hydrogen fuel.

Acknowledgements

J. Demuynck likes to acknowledge the “Institute for the Promotion of Innovation through Science and Technology in Flanders” (IWT-Vlaanderen) for supporting him with a grant (SB-81139). The experimental equipment is funded by a Research Grant (1.5.147.10N) of the “Research Foundation – Flanders” (FWO).

References

[1] Verhelst S. A study of the combustion in hydrogen-fuelled internal combustion engines. Ph.D. Thesis, Ghent University, Ghent, Belgium, 2005. (http://hdl.handle.net/1854/3378).

[2] Demuynck J, Raes N, Zuliani M, De Paepe M, Sierens R, Verhelst S. Local heat flux measurements in a hydrogen and methane spark ignition engine with a thermopile sensor. Int J Hydrogen Energy 2009;34(24):9857–68.

[3] Verhelst S, Sierens R. Combustion studies for PFI hydrogen IC engines. SAE Paper no. 2007-01-3610; 2007.

[4] Verhelst S, De Landtsheere J, De Smet F, Billiouw C, Trenson A, Sierens R. Effects of supercharging, EGR and variable valve timing on power and emissions of hydrogen internal combustion engines. SAE Int J Engines 2009;1(1):647–56 [SAE Paper no. 2008-01-1033; 2008].

[5] Nande AM, Szwaja S, Naber JD. Impact of EGR on combustion processes in a hydrogen fuelled SI engine. SAE Paper no. 2008-01-1039; 2008.

[6] Rottengruber H, Berckmueller M, Elsaesser G, Brehm N, Schwarz C. Direct-injection hydrogen SI-engine operation strategy and power density potentials. Trans SAE, J Fuels Lubricants 2004;113:1749–61 [SAE Paper no. 2004-01-2927].

[7] Verhelst S, Wallner T. Hydrogen-fueled internal combustion engines. Prog Energy Combust Sci 2009;35(6):490–527.

[8] Gerke U. Numerical analysis of mixture formation and combustion in a hydrogen direct-injection internal combustion engine. Ph.D. Thesis, Diss. ETH No. 17477, Cuvillier Göttingen, ETH Zurich, Switzerland, 2007. (http://e-collection.ethbib.ethz.ch/eserv/eth:30102/eth-30102-02.pdf).

[9] Shudo T. Improving thermal efficiency by reducing cooling losses in hydrogen combustion engines. Int J Hydrogen Energy 2007;32(17):4285–93.

[10] Mohammadi A, Shioji M, Nakai Y, Ishikura W, Tabo E. Performance and combustion characteristics of a direct-injection SI hydrogen engine. Int J Hydrogen Energy 2007;32(2):296–304.

[11] Aleiferis PG, Rosati MF. Flame chemiluminescence and OH LIF imaging in a hydrogen-fuelled spark-ignition engine. Int J Hydrogen Energy 2011;37(2):1797–812.

[12] Ohira T, Nakagawa K, Yamane K, Kawanabe H, Shioji M. Experimental study of emission characteristics of a small hydrogen S.I. engine. SAE Paper No. 2007-32-0074; 2007.

[13] Verhelst S, Sierens R. A quasi-dimensional model for the power cycle of a hydrogen-fuelled ICE. Int J Hydrogen Energy 2007;32(15):3545–54.

[14] Safari H, Jazayeri SA, Ebrahimi R. Potentials of NO_X emission reduction methods in SI hydrogen engines: Simulation study. Int J Hydrogen Energy 2009;34(2):1015–25.

[15] Dimopoulos P, Rechsteiner C, Soltic P, Laemmle C, Boulouchos K. Increase of passenger car engine efficiency with low engine-out emissions using hydrogen–natural gas mixtures: A thermodynamic analysis. Int J Hydrogen Energy 2007;32(14):3073–83.

[16] Knop V, Benkenida A, Jay S, Colin O. Modelling of combustion and nitrogen oxide formation in hydrogen-fuelled internal combustion engines within a 3D CFD code. Int J Hydrogen Energy 2008;33(19):5083–97.

[17] Sukumaran S, Kong S-C. Numerical study on mixture formation characteristics in a direct-injection hydrogen engine. Int J Hydrogen Energy 2010;35(15):7991–8007.

[18] Rakopoulos CD, Kosmadakis GM, Demuynck J, De Paepe M, Verhelst S. A combined experimental and numerical study of thermal processes, performance and nitric oxide emissions in a hydrogen-fueled spark-ignition engine. Int J Hydrogen Energy 2011;36(8):5163–80.

[19] Hountalas DT, Mavropoulos GC, Binder KB. Effect of exhaust gas recirculation (EGR) temperature for various EGR rates on heavy duty DI diesel engine performance and emissions. Energy 2008;33(2):272–83.

[20] Pariotis EG, Hountalas DT, Rakopoulos CD. Modeling the effects of EGR on a heavy duty Di diesel engine using a new quasi-dimensional combustion model. SAE Paper No. 2005-01-1125; 2005.

[21] Shin B, Cho Y, Han D, Song S, Chun KM. Hydrogen effects on NO_X emissions and brake thermal efficiency in a diesel engine under low-temperature and heavy-EGR conditions. Int J Hydrogen Energy 2011;36(10):6281–91.

[22] Komninos NP, Rakopoulos CD. Modeling HCCI combustion of biofuels: A review. Renew Sust Energy Rev 2012;16(3):1588–610.

[23] Shi L, Cui Y, Deng K, Peng H, Chen Y. Study of low emission homogeneous charge compression ignition (HCCI) engine using combined internal and external exhaust gas recirculation (EGR). Energy 2006;31(14):2665–76.

[24] Hu E, Huang Z, Liu B, Zheng J, Gu X, Huang B. Experimental investigation on performance and emissions of a spark-ignition engine fuelled with natural gas–hydrogen blends combined with EGR. Int J Hydrogen Energy 2009;34(1):528–39.

[25] Verhelst S, Maesschalck P, Rombaut N, Sierens R. Increasing the power output of hydrogen internal combustion engines by means of supercharging and exhaust gas recirculation. Int J Hydrogen Energy 2009;34(10):4406–12.

[26] Fontana G, Galloni E. Experimental analysis of a spark-ignition engine using exhaust gas recycle at WOT operation. Appl Energy 2010;87(7):2187–93.

[27] Abd-Alla GH. Using exhaust gas recirculation in internal combustion engines: A review. Energy Convers Manage 2002;43(8):1027–42.

[28] Swain MR, Swain MN, Leisz A, Adt RR. Hydrogen peroxide emissions from a hydrogen fueled engine. Int J Hydrogen Energy 1990;15(4):263–6.

[29] Sinclair LA, Wallace JS. Lean limit emissions of hydrogen-fueled engines. Int J Hydrogen Energy 1984;9(1-2):123–28.

[30] Verhelst S, T'Joen C, Vancoillie J, Demuynck J. A correlation for the laminar burning velocity for use in hydrogen spark ignition engine simulation. Int J Hydrogen Energy 2011;36(1):957–74.

[31] Sierens R, Verhelst S. Influence of the injection parameters on the efficiency and power output of a hydrogen fuelled engine. Trans ASME, J Eng Gas Turbines Power 2003;125(2):444–9.

[32] Verhelst S, Sierens R. Combustion strategies and NO_X emissions for hydrogen fuelled IC engines. FISITA, Paper no. F2006.P092, Yokohama, Japan, 2006.

[33] Verhelst S, Verstraeten S, Sierens R. A comparison between lean burn operation and stoichiometric operation with EGR for a hydrogen fuelled IC engine. 16th World Hydrogen Energy Conference (WHEC), Lyon, France, 13-16 June 2006, Paper no. S22-206.

[34] Das LM. Exhaust emission characterization of hydrogen-operated engine system: Nature of pollutants and their control techniques. Int J Hydrogen Energy 1991;16(11):765–75.

[35] Subramanian V, Mallikarjuna JM, Ramesh A. Intake charge dilution effects on control of nitric oxide emission in a hydrogen fueled SI engine. Int J Hydrogen Energy 2007;32(12):2043–56.

[36] Rakopoulos CD, Kosmadakis GM, Pariotis EG. Evaluation of a combustion model for the simulation of hydrogen spark-ignition engines using a CFD code. Int J Hydrogen Energy 2010;35(22):12545–60.

[37] Han Z, Reitz RD. Turbulence modeling of internal combustion engines using RNG k-ε models. Combust Sci Technol 1995;106(4):267–95.

[38] Thakur S, Wright JR. A multiblock operator-splitting algorithm for unsteady flows at all speeds in complex geometries. Int J Numer Methods Fluids 2004;46(4):383–413.

[39] Shyy W. Computational modeling for fluid flow and interfacial transport. Amsterdam: Elsevier Science; 1994.

[40] Rakopoulos CD, Kosmadakis GM, Dimaratos AM, Pariotis EG. Investigating the effect of crevice flow on internal combustion engines using a new simple crevice model implemented in a CFD code. Appl Energy 2011;88(1):111–26.

[41] Rakopoulos CD, Kosmadakis GM, Pariotis EG. Critical evaluation of current heat transfer models used in CFD in-cylinder engine simulations and establishment of a comprehensive wall-function formulation. Appl Energy 2010;87(5):1612–30.

[42] Launder BE, Spalding DB. The numerical computation of turbulent flows. Comput Methods Appl Mech Engrg 1974;3(2):269–89.

[43] Han Z, Reitz RD. A temperature wall function formulation for variable-density turbulent flows with application to engine convective heat transfer modeling. Int J Heat Mass Transfer 1997;40(3):613–25.

[44] Rakopoulos CD, Kosmadakis GM, Pariotis EG. Simulation of a motored internal combustion engine using an improved CFD code, In: Proc of the 23rd Int Conference on Efficiency, Cost, Optimization, Simulation and Environmental Impact of Energy Systems (ECOS 2010), June 14–17, 2010, Lausanne, Switzerland, Paper no. 295.

[45] Rakopoulos CD, Kosmadakis GM, Pariotis EG. Evaluation of a new computational fluid dynamics model for internal combustion engines using hydrogen under motoring conditions. Energy 2009;34(12):2158–66.

[46] Gerke U, Steurs K, Rebecchi P, Boulouchos K. Derivation of burning velocities of premixed hydrogen/air flames at engine-relevant conditions using a single-cylinder compression machine with optical access. Int J Hydrogen Energy 2010;35(6):2566–77.

[47] Zimont VL. Gas premixed combustion at high turbulence. Turbulent flame closure combustion model. Exp Therm Fluid Sci 2000;21(1-3):179–86.

[48] Lipatnikov AN, Chomiak J. A simple model of unsteady turbulent flame propagation. Trans SAE, J Engines 1997;106:2441–52 [SAE Paper no. 972993].

[49] Bleechmore C, Brewster S. Dilution strategies for load and NO_X management in a hydrogen fuelled direct injection engine. SAE Paper no. 2007-01-4097; 2007.

[50] Abraham J, Bracco FV, Reitz RD. Comparison of computed and measured premixed charge engine combustion. Combust Flame 1985;60(3):309–22.

[51] Fan L, Reitz RD. Development of an ignition and combustion model for spark-ignition engines. Trans SAE, J Engines 2000;109:1977–89 [SAE Paper no. 2000-01-2809].

[52] Masood M, Ishrat MM, Reddy AS. Computational combustion and emission analysis of hydrogen-diesel blends with experimental verification. Int J Hydrogen Energy 2007;32(13):2539–47.

[53] Kong S-C, Ayoub N, Reitz RD. Modeling combustion in compression ignition homogeneous charge engines. Trans SAE, J Engines 1992;101:896–911 [SAE Paper no. 920512].

[54] Lavoie GA, Heywood JB, Keck JC. Experimental and theoretical study of nitric oxide formation in internal combustion engines. Combust Sci Technol 1970;1(4):313–26.

[55] Rakopoulos CD, Michos CN. Development and validation of a multi-zone combustion model for performance and nitric oxide formation in syngas fueled spark ignition engine. Energy Convers Manage 2008;49(10):2924–38.

[56] Heffel JW. NO_X emission and performance data for a hydrogen fueled internal combustion engine at 1500 rpm using exhaust gas recirculation. Int J Hydrogen Energy 2003;28(8):901–8.

[57] Fox JW, Cheng WK, Heywood JB. A model for predicting residual gas fraction in spark-ignition engines. Trans SAE, J Engines 1993;102:1538–44 [SAE Paper no. 931025].

[58] Senecal PK, Xin J, Reitz RD. Predictions of residual gas fraction in IC engines. Trans SAE, J Engines 1996;105:2243–54 [SAE Paper no. 962052].

[59] Shudo T, Nabetani S. Analysis of degree of constant volume and cooling loss in a hydrogen fuelled SI engine. Trans SAE, J Fuels Lubricants 2001;110:1911–17 [SAE Paper no. 2001-01-3561].

[60] Obermair H, Scarcelli R, Wallner T. Efficiency improved combustion systems for hydrogen direct injection operation. SAE Paper no. 2010-01-2170; 2010.

Tables Captions

Table 1 CFR engine specifications.

Table 2 Test cases examined in the present study.

Table 3 Coefficients (c_i) of Eq. (8) [30].

Table 1. - CFR engine specifications.

Engine model and type		CFR engine, single cylinder, naturally aspirated, four-stroke, water-cooled
Bore		82.55 mm
Stroke		114.2 mm
Swept volume		0.6117 lit
Connecting rod length		254 mm
Compression ratio		9:1
Valves		2 (unshrouded)
Engine speed		600 rpm (constant)
Ignition timing		MBT
End of port-fuel injection (intake stroke)		BDC
Injection pressure (gauge)		2 bar
Number of piston rings		5
Valve timing events	Inlet valve opening	17 ^{o}CA ATDC
	Inlet valve closure	26 ^{o}CA ABDC
	Exhaust valve opening	32 ^{o}CA BBDC
	Exhaust valve closure	6 ^{o}CA ATDC

Table 2. - Test cases examined in the present study.

Case	EGR percentage (% by mass)	MBT timing (^{o}CA ABDC)	H_2 flow rate (Nm^3/h)
1	12.87	185.5	2.275
2	18.92	182.4	2.099
3	26.94	178.7	1.971
4	34.49	172.0	1.802
5	42.15	171.7	1.638
6	47.47	170.0	1.477

Table 3. - Coefficients c_i of Eq. (8) [30].

Coefficient (i=1-10)	Value	Coefficient (i=11-21)	Value
c_1	1.782191	c_{11}	3.724404E-03
c_2	-1.945813E-01	c_{12}	-2.114637E-01
c_3	-4.071734E-03	c_{13}	-2.224738E-01
c_4	-4.987061E-01	c_{14}	4.624703E-02
c_5	-4.347767	c_{15}	2.116186E-01
c_6	8.576177E-05	c_{16}	-2.098941
c_7	4.490150E-02	c_{17}	7.029643E-02
c_8	7.878902E-02	c_{18}	1.334951
c_9	4.243647	c_{19}	4.861730E-04
c_{10}	-2.052509E-03	c_{20}	-1.915344E-02
		c_{21}	6.146191E-01

Figures Captions

Fig. 1 - Engine test-rig with the exhaust gas recirculation (EGR) line.

Fig. 2 - Measured hydrogen flow rates for the two strategies of variable EGR or mixture leaning.

Fig. 3 - Coefficient of variance (COV) of indicated mean effective pressure (IMEP) for the two strategies of variable EGR or mixture leaning.

Fig. 4 - Comparison of the calculated values of the residual gas term 'F' previously used [1] and the new one [30], for three combinations of pressure and unburned gas temperature, and two equivalence ratios.

Fig. 5 - Calculated NO mass fraction at EVO as a function of successive (multiple) simulation cycles, for two EGR rates (26.94 and 47.47%).

Fig. 6 - Computational grid used, depicting the location of the spark-plug (off-set from the cylinder axis).

Fig. 7 - Comparison of calculated cylinder pressures and net heat release rates with the measured ones for various EGR rates.

Fig. 8 - Comparison of calculated gross indicated mean effective pressure (IMEP) and indicated efficiency with the measured ones for various EGR rates.

Fig. 9 - Comparison of calculated exhaust nitric oxide (NO) emissions with the measured ones for various EGR rates.

Fig. 10 Temperature and NO mass fraction spatial distributions during the combustion period for three EGR rates (Cases 2, 4, 6 of Table 2).

Fig. 11 - Calculated hydrogen mass fraction burned for various EGR rates.

Fig. 12 - Combustion durations of 0-5%, 5-99% and 0-99% mass fractions burned (MFB) for various EGR rates.

Fig. 13 - Calculated unburned hydrogen (% vol.) at the exhaust for various EGR rates.

Fig. 14 - Laminar and turbulent flame speeds of the mixture, located at the axial direction crossing the spark-plug for various EGR rates.

Fig. 15 - Flame radius for various EGR rates.

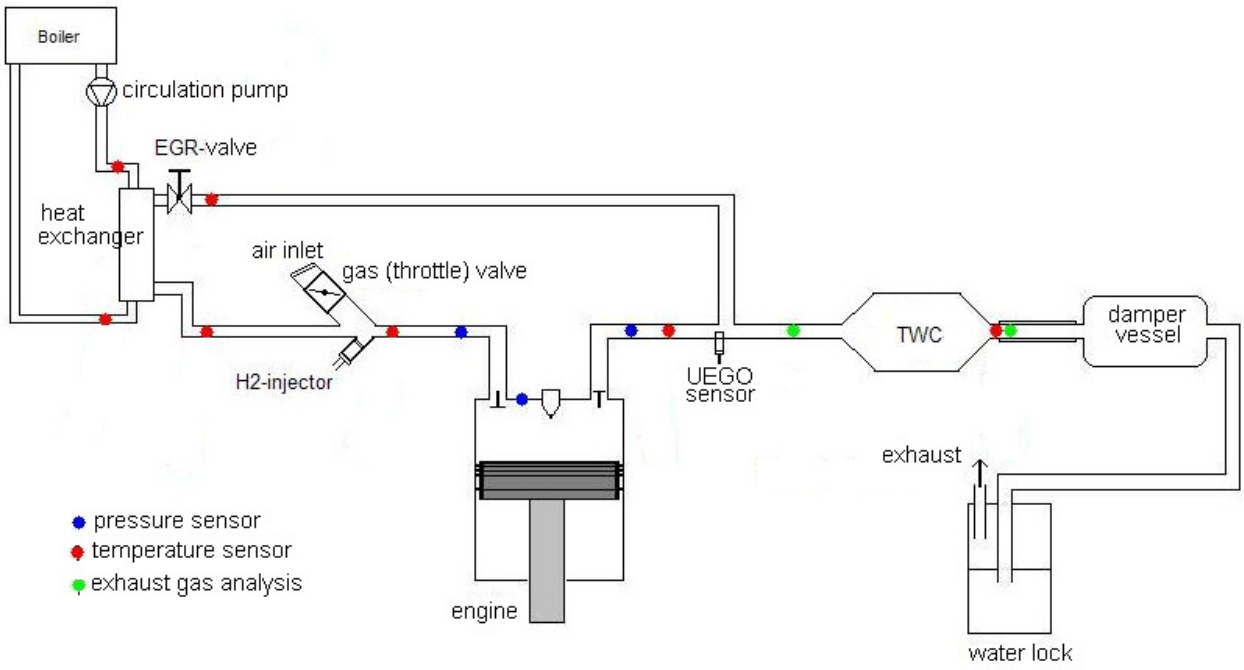

Fig. 1 Kosmadakis et al.

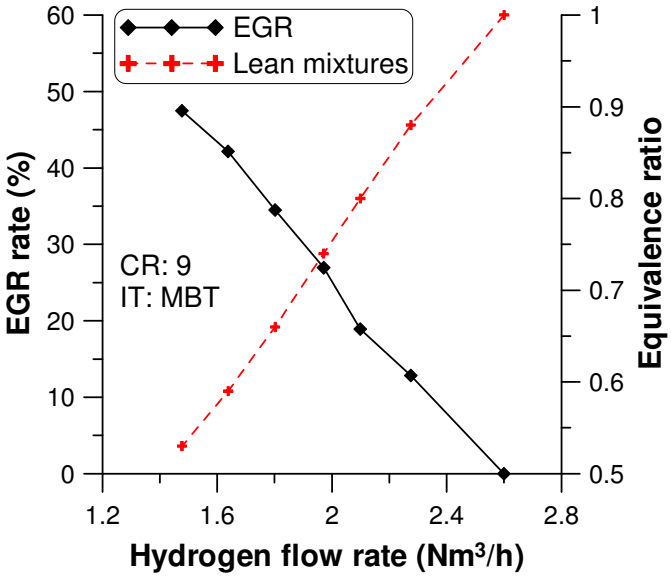

Fig. 2 Kosmadakis et al.

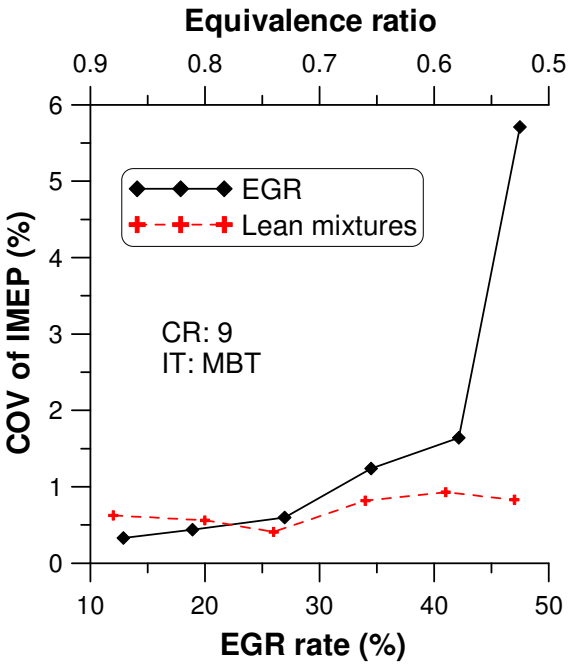

Fig. 3 Kosmadakis et al.

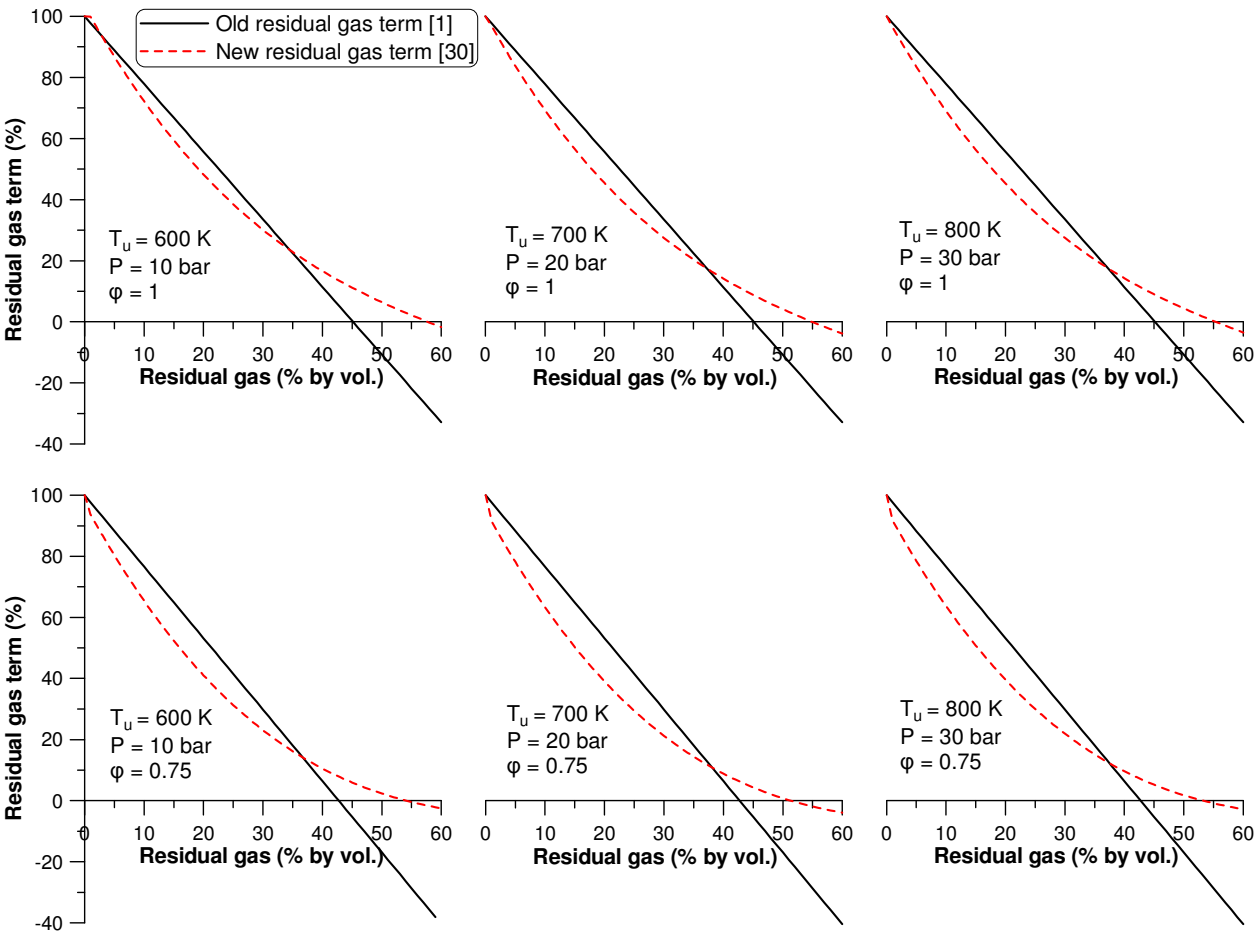

Fig. 4 Kosmadakis et al.

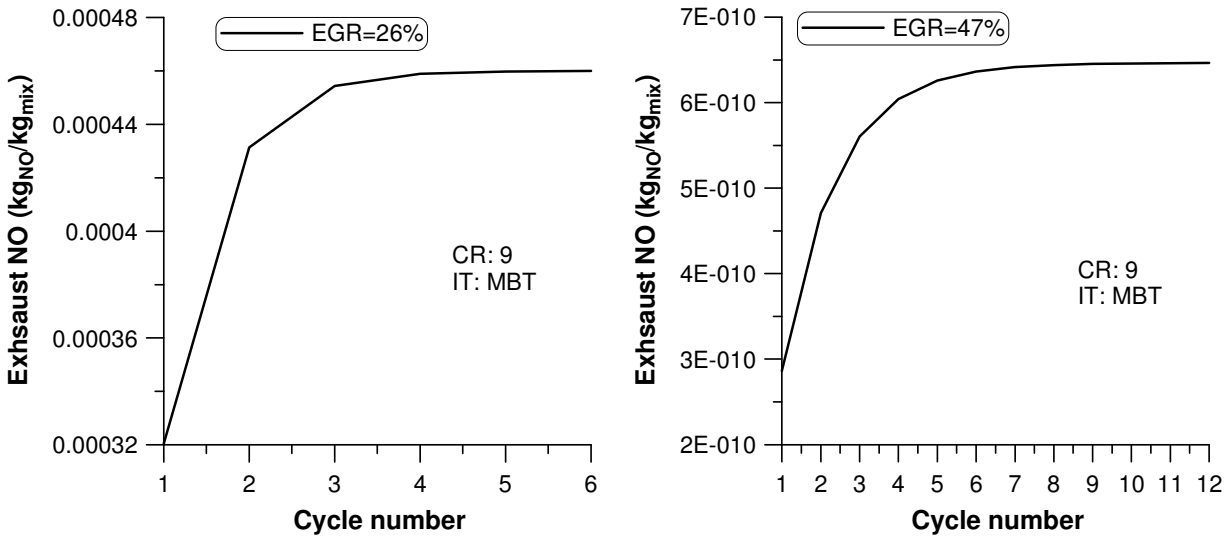

Fig. 5 Kosmadakis et al.

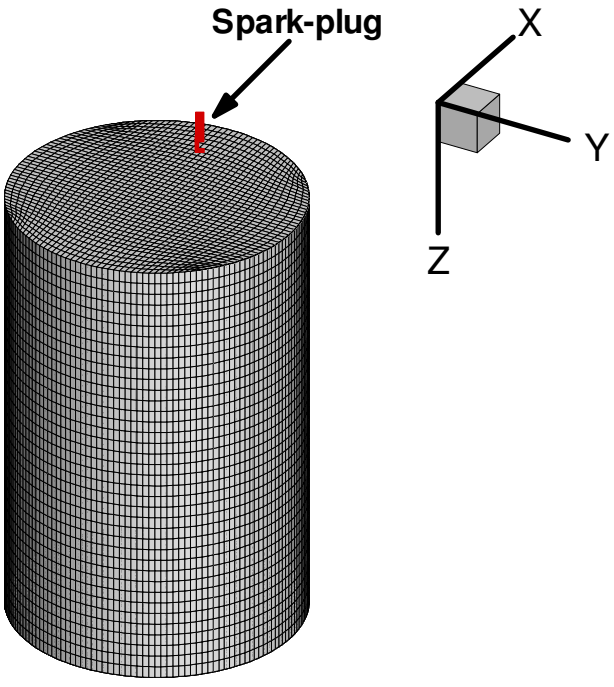

Fig. 6 Kosmadakis et al.

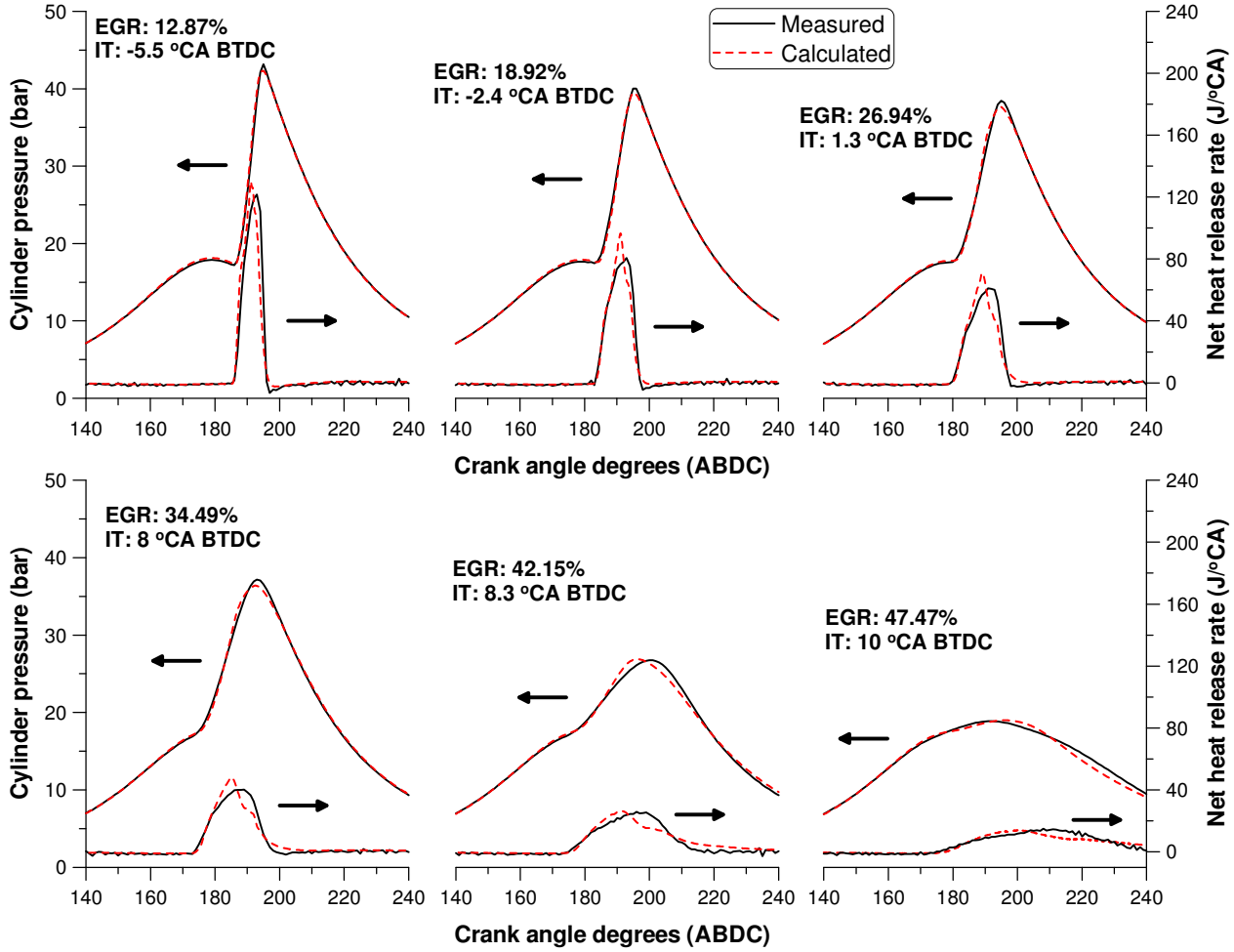

Fig. 7 Kosmadakis et al.

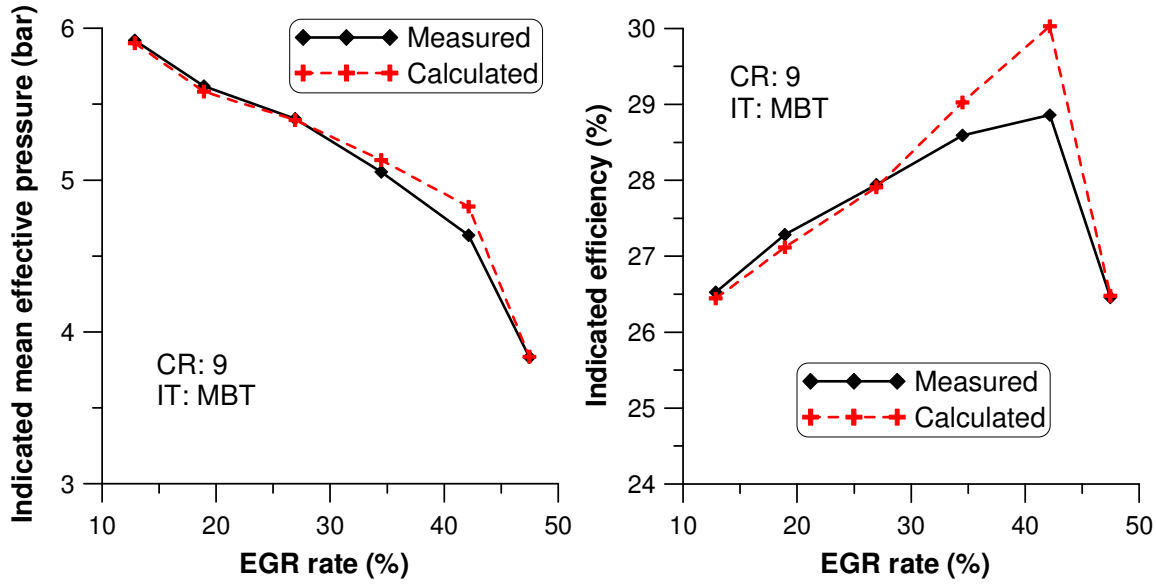

Fig. 8 Kosmadakis et al.

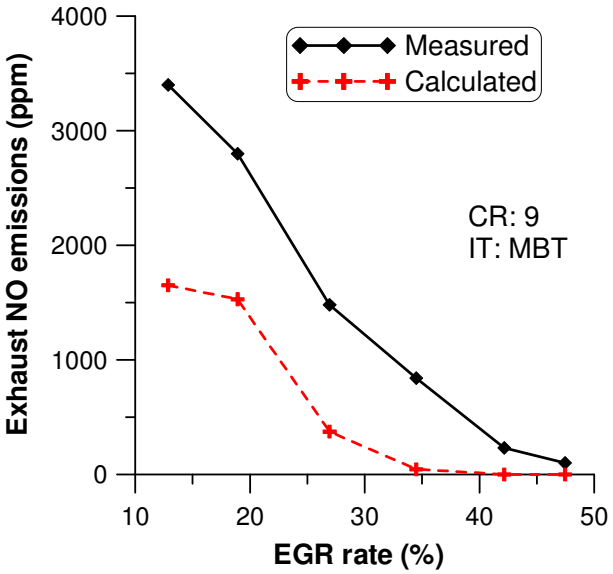

Fig. 9 Kosmadakis et al.

°CA after IT	EGR=18.92%	EGR=34.49%	EGR=47.47%
8	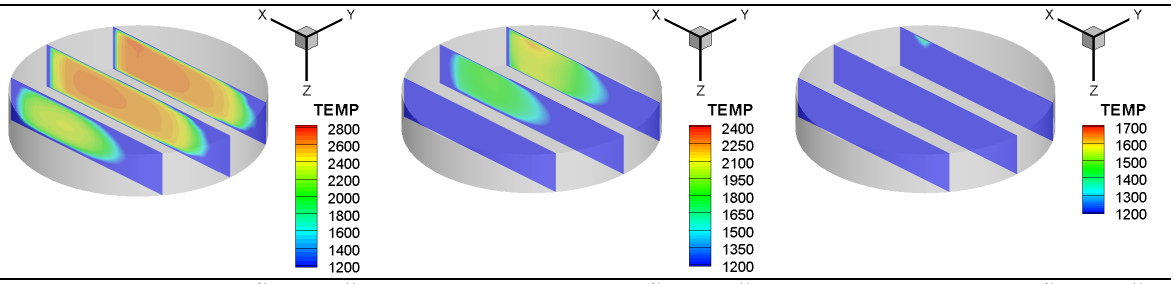	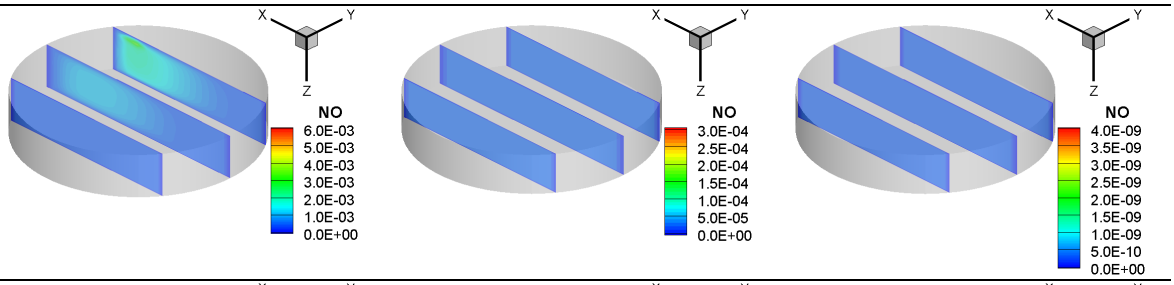
20	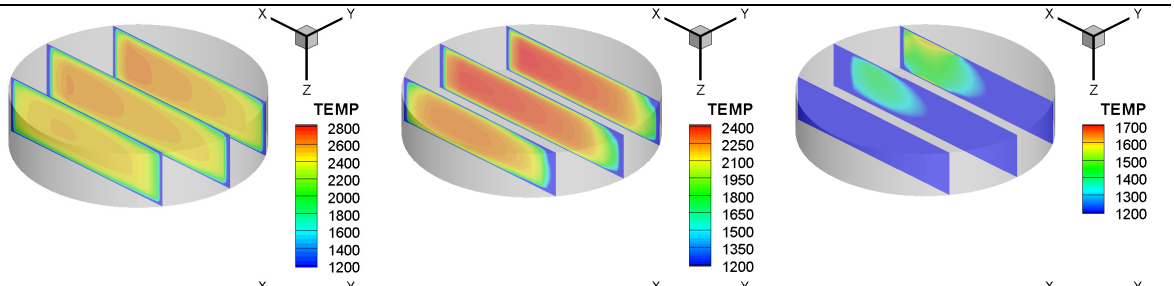	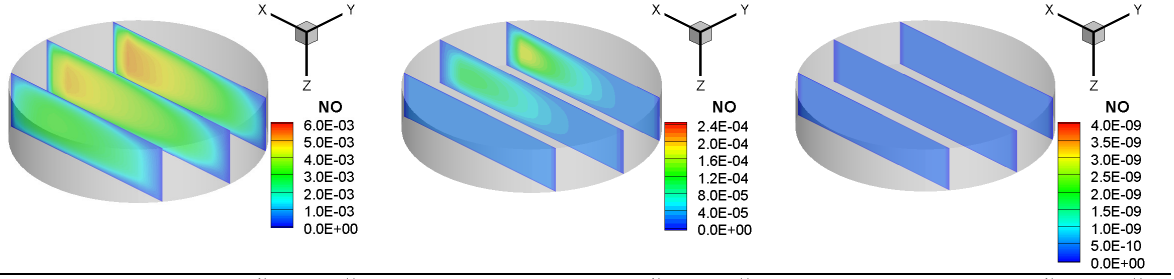
32	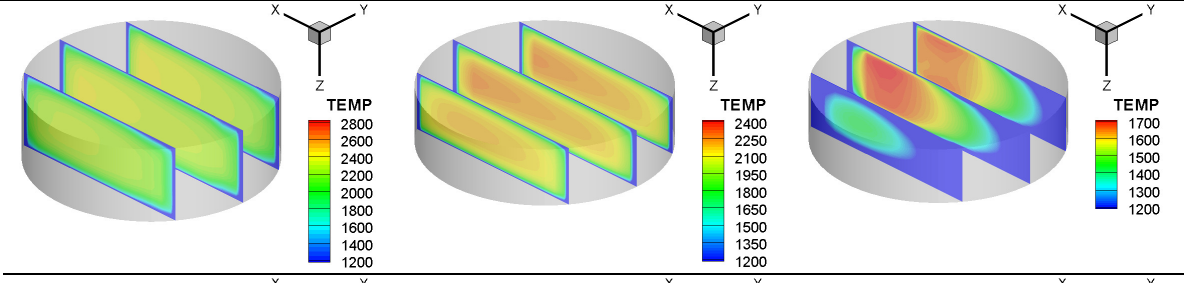	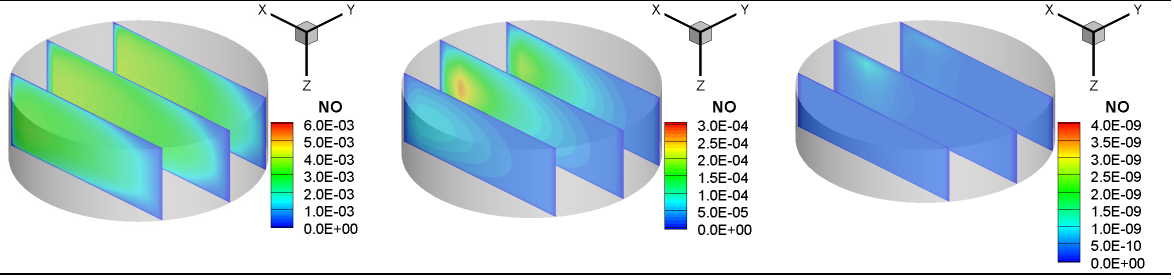

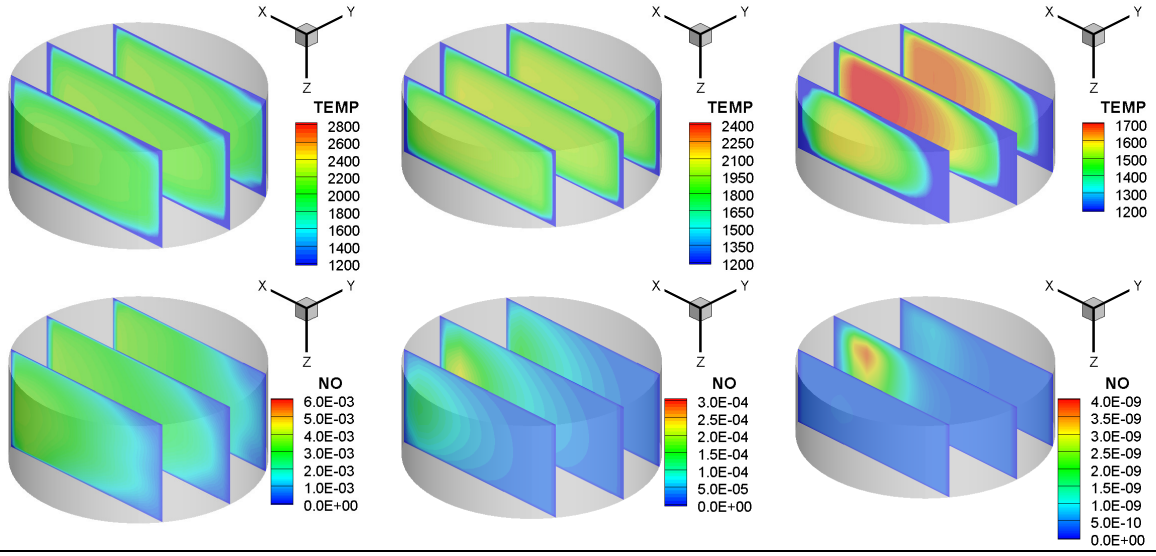

Fig. 10 Kosmadakis et al.

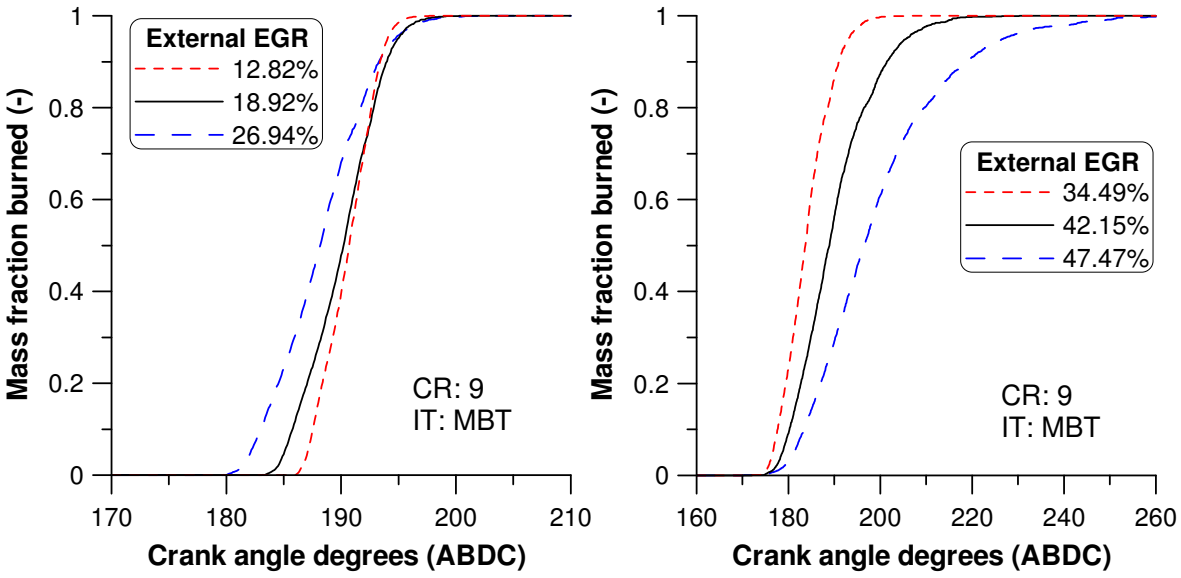

Fig. 11 Kosmadakis et al.

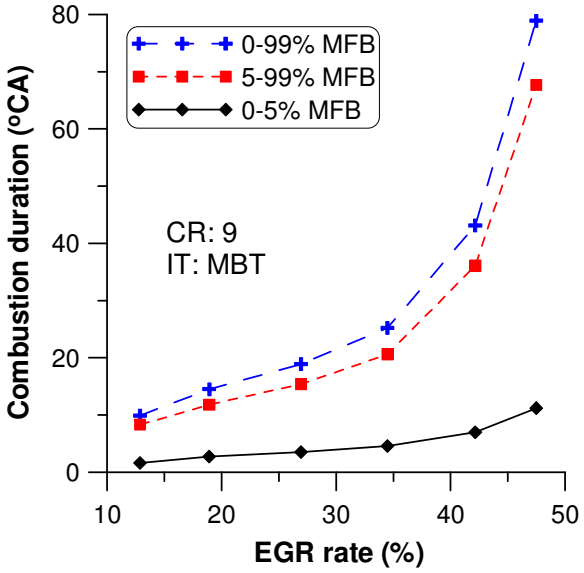

Fig. 12 Kosmadakis et al.

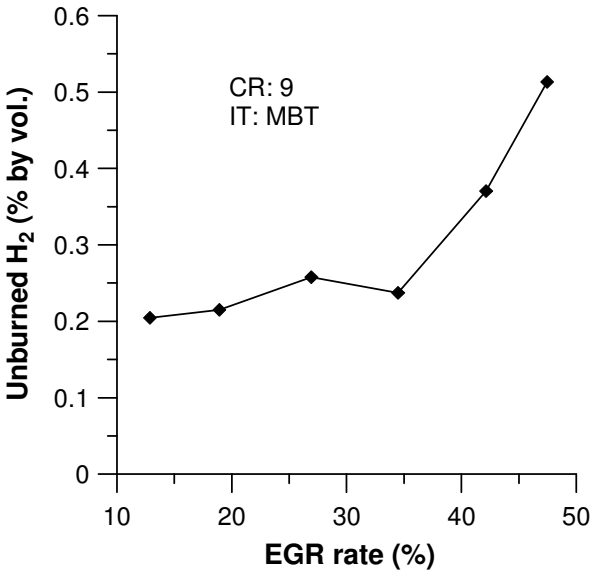

Fig. 13 Kosmadakis et al.

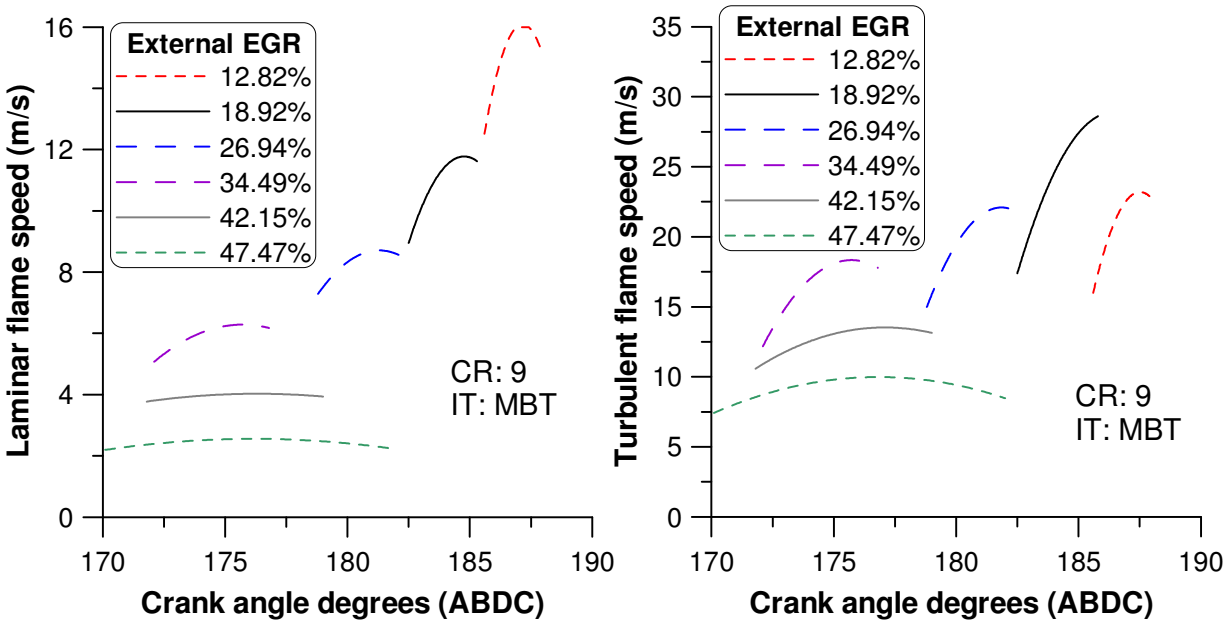

Fig. 14 Kosmadakis et al.

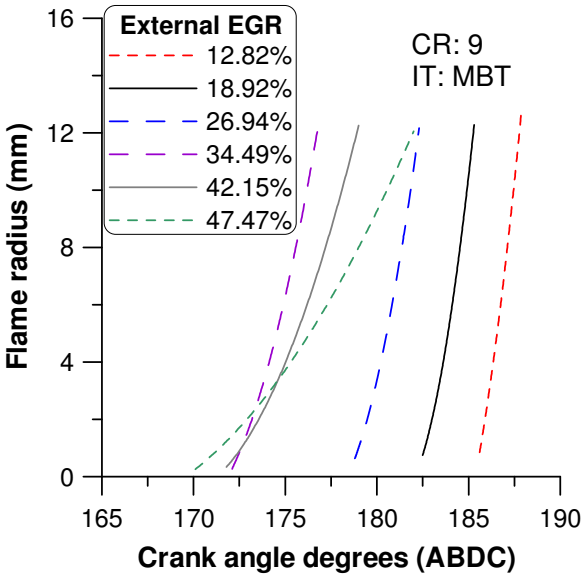

Fig. 15 Kosmadakis et al.